



Prediction of Mooring System Characteristics of the Floating Barge using Deep Neural Networks

Janghoon Seo

Shipbuilding & Marine Simulation Center, Tongmyong University, Busan, Republic of Korea

Dong-Woo Park

Autonomous Vehicle System Engineering Major, School of Electrical and Control Engineering, Tongmyong University, Busan, Republic of Korea, dwpark@tu.ac.kr

Follow this and additional works at: <https://jmstt.ntou.edu.tw/journal>



Part of the [Fresh Water Studies Commons](#), [Marine Biology Commons](#), [Ocean Engineering Commons](#), [Oceanography Commons](#), and the [Other Oceanography and Atmospheric Sciences and Meteorology Commons](#)

Recommended Citation

Seo, Janghoon and Park, Dong-Woo (2024) "Prediction of Mooring System Characteristics of the Floating Barge using Deep Neural Networks," *Journal of Marine Science and Technology*. Vol. 32: Iss. 3, Article 4.

DOI: 10.51400/2709-6998.2745

Available at: <https://jmstt.ntou.edu.tw/journal/vol32/iss3/4>

This Research Article is brought to you for free and open access by Journal of Marine Science and Technology. It has been accepted for inclusion in Journal of Marine Science and Technology by an authorized editor of Journal of Marine Science and Technology.

RESEARCH ARTICLE

Prediction of Mooring System Characteristics of the Floating Barge Using Deep Neural Networks

Janghoon Seo ^a, Dong-Woo Park ^{b,*}

^a Shipbuilding & Marine Simulation Center, Tongmyong University, Busan, Republic of Korea

^b Autonomous Vehicle System Engineering Major, School of Electrical and Control Engineering, Tongmyong University, Busan, Republic of Korea

Abstract

The present study establishes deep learning models to predict the tensions and inclinations of mooring lines of a floating barge and verifies applicability of these models. Hydrodynamic and mooring analyses are conducted on the dataset used for the deep learning models. Three types of neural network models include a deep neural network (DNN) with input data representing the 6° of freedom motions of a floating barge, convolutional neural network (CNN) with input images of the floating barge and mooring lines on a horizontal plane, and hybrid neural network (HNN) that consolidates the characteristics of DNN and CNN models. The output labels for the deep learning models are the tension and inclination of each mooring line. The models are trained using various hyperparameters, and the effect of the hyperparameters on model performance is investigated. The accuracy of the established models is evaluated through testing. The test results indicate that the DNN and HNN models outperform the CNN model, which is constrained by its dependency on two-dimensional image input data. The DNN and HNN models are able to accurately predict the mooring line tension and inclination under various environmental conditions, except for several peaks in harsh environments. The present study shows that the established deep learning models have the potential to replace a mooring monitoring system with fast and accurate predictions. Further research is required to investigate their applicability in mooring systems with multiple mooring lines and turret mooring systems.

Keywords: Deep learning model, Floating barge, Mooring system analysis

1. Introduction

Floating offshore structures maintain their positions by the position keeping systems for safe operation. The mooring system is one of the most widely used position keeping systems. This system maintains the position of a floating structure using the weight and elasticity of mooring lines. The mooring system requires the monitoring system to ensure a safe operation [1,2]. A typical mooring monitoring system is designed to measure the tension and inclination using sensors at the fairlead. Additionally, an auxiliary monitoring system is required to prepare for equipment malfunction. It derives the tension and inclination of mooring lines

based on the position of a floating structure obtained from mooring system analysis. Thus a mooring system analysis is essential for the design of mooring and monitoring systems.

Various previous researches have been conducted on the analysis of mooring systems. The analysis generally considers the effects of environmental conditions, hydrodynamic performance, and mooring system characteristics. Ormberg and Larsen [3] compared the results of coupled and uncoupled mooring analyses and concluded that the coupled analysis provides more accurate results and better agrees with the model test results than those from the uncoupled analysis. Low and Langley [4] performed a mooring analysis with the coupling of a

Received 8 March 2024; revised 24 June 2024; accepted 3 July 2024.
Available online 20 September 2024

* Corresponding author.
E-mail address: dwpark@tu.ac.kr (D.-W. Park).



hull, riser, and mooring system in the linearized frequency domain. Linearized drag forces on the risers and mooring lines provided good agreement between results of analysis based on the frequency and time domains.

In addition to the previous researches on coupling effects, researches on mooring analysis, altering the model of the mooring line, and the effect on extreme value estimation have been conducted. Garret [5] introduced the three-dimensional finite element methods (FEM) which accounts for large deflections and finite rotations with tension variation along the line length. Davids and Mungall [6] proposed a mooring analysis in the frequency domain with simple equivalent springs. Their result was compared with that of the FEM and significant differences were found. Kim et al. [7] applied linear and nonlinear FEM methods in a coupled mooring analysis. The effect of the coupling stiffness of the mooring system was remarkable when the wave drift forces were large and the weight of the mooring system is not negligible. Va'zquez et al. [8] compared the methodology of the extreme value analysis of Weibull fitting, square root of the sum of the squares, and linear sum. Among the extreme value methodologies, the approach of the square root of the sum of the squares underestimates the extreme values. Staniscic et al. [9] assessed the methodology of extreme response and the effect of the number of realizations. Sagrilo et al. [10] investigated the effect of extreme methodology with varying simulation times. Their results implied that the Weibull approach relatively provides good agreement and convergence depending on the length of simulation time.

Mooring system analysis requires the high techniques, computational equipment, and significant time. To overcome these burdens, recent researches have focused on predicting the performance of mooring systems using deep learning technology. Simoes et al. [11] predicted the tensions of mooring lines and hawsers between floating production storage and offloading (FPSO) vessel and shuttle tanker in a tandem mooring system. A neural network model was applied to predict complex dynamics for the FPSO tandem mooring system. Guarize et al. [12] suggested a hybrid artificial neural network (ANN) – FEM to perform dynamic analysis of mooring lines and risers. The ANN-FEM methodology provided faster performance for a long response of time histories than a complete simulation. Furthermore, de Pina et al. [13] compared the performances between ANN and the wavelet network (WN). The mooring line tensions and motion of the floating production system (FPS) were

compared among the results of FEM, ANN, and WN. They suggested that the ANN and WN approaches exhibited a rapid and inexpensive prediction compared to the FEM. In addition, de Pina et al. [14] expanded their research for the prediction of the offset and tensions of the mooring system of an FPS by using an ANN method. The azimuth, horizontal distance between the anchor and fairlead, and pretension and diameter of the mooring components were selected as input variables with lower and upper bounds under fixed environmental conditions. Fairly accurate prediction results were achieved for the offsets and tension by comparing them with the results of a mooring analysis. Christiansen et al. [15] suggested several error functions for an ANN and applied these error functions instead of a general error function. The application of a weighted error function provided improved prediction by the ANN. Mentés et al. [16] compared an ANN and adaptive neuro-fuzzy inference system (ANFIS) for a tanker-buoy mooring system. Results of ANN and ANFIS showed reliable accuracies and applicability for the mooring analysis. In addition to the aforementioned researches, several previous researches have been conducted to predict the performance of mooring systems using deep learning methodology [17–19].

Deep learning techniques have been used to predict the damage of mooring lines. Chung et al. [20] predicted the classification of a damaged mooring line using deep neural networks (DNN). They expanded their research using a recurrent neural network (RNN) to detect the damage of mooring lines [21]. The number of hidden layers was adjusted and the results of the RNN model were compared with those of a mooring analysis. Another study of the detection of mooring line failure was performed by Saad et al. [22]. The methodologies of multilayer perceptron (MLP) and long short-term memory (LSTM) were applied in their study of prediction on the motion with mooring line breakage. The result of LSTM showed better predictions of the motion of the platform than that of MLP.

Through these previous research efforts, the accuracy of mooring system analysis has been improved and the applicability of deep learning methodology to mooring system has been investigated. However, these researches on mooring system analysis have mainly focused on improving accuracy and refinement of methodologies. In earlier researches addressing the detection of damaged lines [20,21], there are limitations related to the time marching problem and only the classification of mooring line damage is predicted.

The auxiliary mooring monitoring system relies on expensive analysis software and high-

performance computers, incurring high maintenance costs throughout the 20-year design life of floaters. Additionally, software malfunctions necessitate the presence of engineers onboard for maintenance, creating unnecessary burdens. For these reasons, research is needed to confirm the potential of deep learning models in replacing the mooring analysis software used in auxiliary mooring monitoring systems. Additionally, research is required on the accuracy of deep learning model predictions based on the information obtained from the navigator or sensors at operating sites.

In this study, we establish deep learning models to predict the mooring line tension and inclination of a mooring monitoring system. To achieve this, we utilize images of the floating structure in the horizontal plane, typically displayed on navigation monitors, along with position information from the sensors of the ship as input data. Three deep learning models are trained by varying the hyperparameters. Subsequently, the tensions and inclinations of the mooring lines are predicted using the established models. Additionally, we evaluate the applicability of these models under different environmental conditions, which were not used during their establishment. Through this, we aim to verify the feasibility of utilizing the deep learning models in a mooring monitoring system.

2. Mooring system and environmental conditions

2.1. Floating barge and mooring system

In the present study, typical barge is applied as shown in Fig. 1 [23]. The length between perpendiculars, breadth and draft are 150.0 m, 50.0 m and 10.0 m, respectively. Detailed information for the barge is presented in Table 1. A right-handed coordinate system based on the midship, center line and draft, is applied as shown in Fig. 2.

A spread mooring system with four mooring lines are considered. The mooring system is symmetric about the x- and y-axes. The mooring lines are defined as ML1, ML2, ML3, and ML4 as shown in



Fig. 1. Hull shape of floating barge.

Table 1. Main particulars of floating barge.

| Item | Symbol | Value | Unit |
|------------------------------------|----------|--------|----------------|
| Length between perpendicular | LBP | 150.0 | m |
| Breadth | B | 50.0 | m |
| Draft | d | 10.0 | m |
| Displaced volume | Δ | 73,750 | m ³ |
| Radius of gyration in roll motion | Kxx | 20.0 | m |
| Radius of gyration in pitch motion | Kyy | 39.0 | m |
| Radius of gyration in yaw motion | Kzz | 39.0 | m |

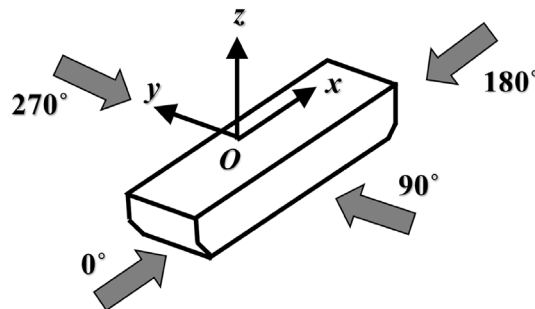
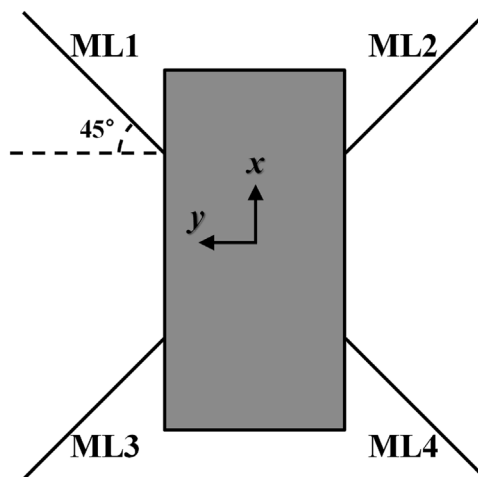
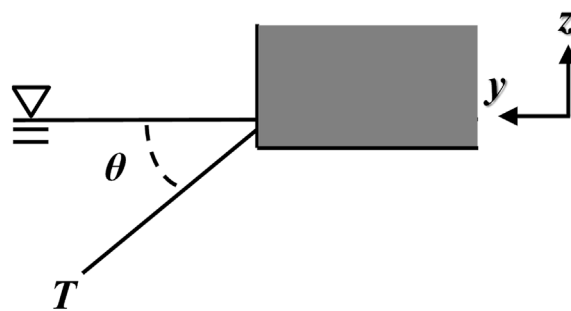


Fig. 2. Coordinate system.



(a)



(b)

Fig. 3. Definition of mooring system. (a) Mooring system configuration. (b) Axial tension and inclination.

Fig. 3(a). The fairleads are close to the corners of the barge. A line orientation with 45° for each mooring line is considered. The axial tension and inclination from the horizontal plane of the mooring line are defined in Fig. 3(b). The horizontal distance between the anchor and fairlead is selected to 1000 m. The water depth is considered to be 1500 m with a flat seabed. The positions of the anchor and the fairlead are presented in Table 2. The mooring line is composed of top chain attached to the fairlead, mid wire, and bottom chain attached to the anchors. The length, diameter, weight and minimum breaking load for each component is shown in Table 3. Each mooring line has the same component and length.

2.2. Environmental conditions

Wave, wind, and current environmental conditions are considered to perform the mooring system analysis and establish the deep learning dataset, as shown in Table 4. The wave and wind are modeled using the Joint North Sea Wave Project (JONSWAP) and American Petroleum Institute (API) spectra, respectively. A long-crested wave is assumed without a spreading function. A steady current with a constant velocity profile along to water depth is considered. An omni-directional environmental condition is considered, in which the wave, wind, and current come from the same direction.

Table 2. Fairlead and anchor locations.

| Line | Fairlead | | | Anchor | | |
|------|--------------------|------------------------|------------------|--------------------|-----------------------|------------------|
| | x from midship (m) | y from center line (m) | z from draft (m) | x from midship (m) | y from centerline (m) | z from draft (m) |
| ML1 | 50.0 | 25.0 | -2.5 | 757.107 | 732.107 | -1500.0 |
| ML2 | 50.0 | -25.0 | -2.5 | 757.107 | -732.107 | -1500.0 |
| ML3 | -50.0 | 25.0 | -2.5 | -757.107 | 732.107 | -1500.0 |
| ML4 | -50.0 | -25.0 | -2.5 | -757.107 | 732.107 | -1500.0 |

Table 3. Mooring line components.

| Item | Type | Length (m) | Diameter (mm) | Weight in water (kg/m) | Minimum Breaking load (kN) |
|--------------|--------------------|------------|---------------|------------------------|----------------------------|
| Top chain | R4 studless | 100 | 105 | 241.448 | 10,754 |
| Mid wire | Spiral strand wire | 1500 | 102 | 57.400 | 10,790 |
| Bottom chain | R4 studless | 200 | 105 | 241.448 | 10,754 |

Table 4. Environmental conditions.

| Item | Wave | | Wind velocity | Current velocity | Direction from |
|------|--------|--------|---------------|------------------|----------------|
| | Hs (m) | Tp (s) | Vw (m/s) | Vc (m/s) | (°) |
| ENV1 | 1.5 | 6.5 | 7.5 | 0.5 | 0.0–90.0 |
| ENV2 | 2.5 | 8.5 | 11.5 | 0.9 | 15.0 interval |
| ENV3 | 3.5 | 10.5 | 15.5 | 1.3 | |
| ENV4 | 0.5 | 4.5 | 3.5 | 0.1 | 0, 45, 90 |
| ENV5 | 2.0 | 7.5 | 9.5 | 0.7 | |
| ENV6 | 5.0 | 12.5 | 20.5 | 1.7 | |

To establish the deep learning model, ENV1, ENV2, and ENV3 are employed with environmental directions from 0° to 90° with an interval of 15°. ENV4, ENV5, and ENV6 are selected as benign, median, and harsh conditions, respectively, compared with ENV1, ENV2 and ENV3. ENV4, ENV5 and ENV6 are used to evaluate the additional performance of the established deep learning models. The directions of ENV4, ENV5, and ENV6 are 0°, 45°, and 90°.

3. Preparation of dataset by hydrodynamic and mooring analysis

To prepare the dataset of the deep learning models, the hydrodynamic analysis is performed to derive the first order motion, second order wave drift force, added mass, and the response amplitude operator (RAO) of first order motions. The general equation of motion in 6° of freedom (6-DOF) for the barge based on the time domain is presented below.

$$(M + A)\ddot{\zeta}_i(t) + B\dot{\zeta}_i(t) + C\zeta_i(t) + \int_0^t R(t - \tau)\dot{\zeta}_i(t)d\tau = F_i(t) \tag{1}$$

where, t , ζ_i , and F_i represent the time, body motion, and external force, respectively. M , A , B , C and R are

the mass, added mass, damping, stiffness and memory function, respectively.

The mooring line analysis for the barge is performed based on catenary line characteristic solution in the time domain. The general equations of catenary calculation are presented below.

$$S - S_0 = \frac{H}{w} \sinh^{-1} \left(\frac{wL}{H} \right) - \frac{H_0}{W} \sinh^{-1} \left(\frac{wL_0}{H_0} \right) + \frac{L_T}{AE} (H - H_0) - (L - L_0) \quad (2)$$

$$H = AE \sqrt{\left(\frac{T}{AE} + 1 \right)^2 - \frac{2wh}{AE}} - AE; L = \frac{1}{w} \sqrt{T^2 - H^2} \quad (3)$$

$$H_0 = AE \sqrt{\left(\frac{T_0}{AE} + 1 \right)^2 - \frac{2wh}{AE}} - AE; L_0 = \frac{1}{w} \sqrt{T_0^2 - H_0^2} \quad (4)$$

where, H , H_0 , T and T_0 are horizontal tension, initial horizontal tension, axial tension, and initial axial tension, respectively. w is submerged unit weight of mooring line and h is water depth. AE is the multiplication of cross-sectional area and elasticity of the mooring line. L is the total length of the mooring line underwater and L_T is the upstretched length of the mooring line.

Hydrodynamic and mooring analyses are performed by Ansys AQWA which is based on three-dimensional radiation and diffraction approaches. Wind and current force coefficients are applied based on the definition from the Oil Companies International Marine Forum (OCIMF) [24]. Low-frequency linear damping coefficients are applied from Bureau Veritas (BV) [25]. A three-dimensional hydrodynamic panel model and mooring system are presented in Fig. 4. The total simulation time is 12800 s with a time step of 0.1 seconds. The first 2000 s is not considered in the dataset of the deep learning model to remove the transient effect. To validate the hydrodynamic model and configuration, the results of the hydrodynamic analysis for the first order response amplitude operator (RAO) and mean drift forces in the surge and sway directions are compared with those of previous researches as shown in Fig. 5 [23,26].

The results of the mooring system analysis used as the dataset for the deep learning model are assessed. The variations in the maximum offset of the floating barge and the maximum tensions of the mooring lines under different environmental conditions are shown in Fig. 6. The maximum offset is observed when the environmental load is applied

from the side of the floating barge, as shown in Fig. 6(a). This can be attributed to an increase in the environmental load due to an increase in the projection area. For the mooring line tensions, ML2 and ML4 show the highest tension when the environmental condition direction is 90° because these are located in the direction of the environmental load, as shown in Fig. 6(b). On the other hand, ML1 and ML3 are located in the opposite direction to the environmental condition from the side, resulting in a lower tension. An increase in the magnitude of the environmental load intensifies the directional variations in the offset and mooring line tension. This is attributed to the relationship between the environmental load and the magnitude of wave height, wind velocity and current velocity.

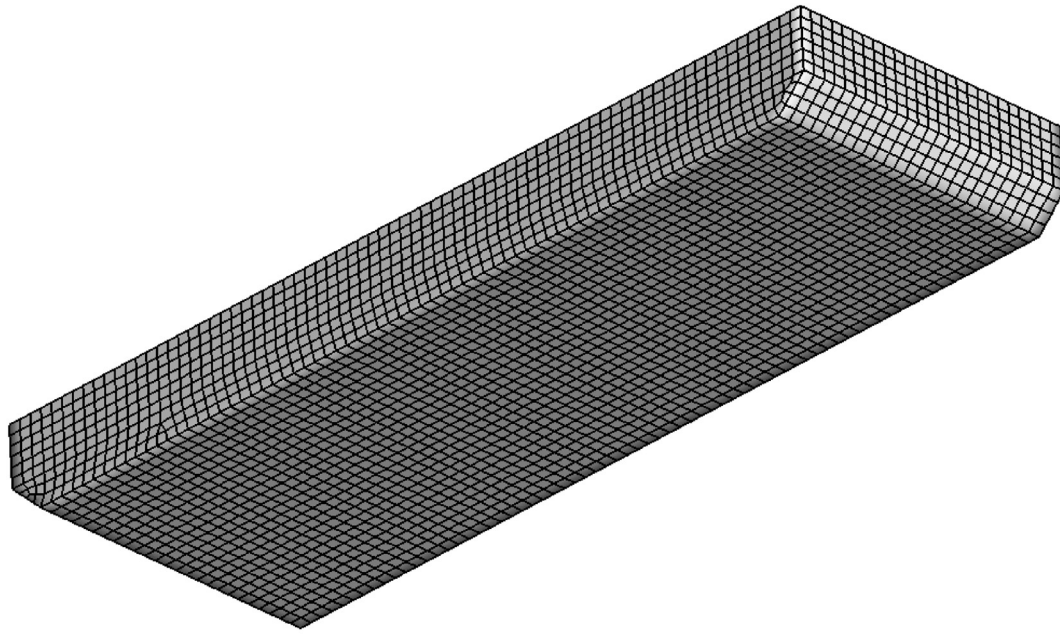
4. Deep learning model

In the present study, both DNN and CNN are utilized. Additionally, a hybrid deep learning model that integrates DNN and CNN models is employed and referred to as HNN. Typical architectures of the three models are presented in Fig. 7. The DNN architecture contains multiple hidden layers to train and test the mooring line responses. Each layer consists of multiple neurons, and each neuron is connected to the neurons in the adjacent layer. The DNN architecture is generally composed of input, hidden, and output layers as shown in Fig. 7(a). Input data is fed into the input layer, which processes it and passes it to the hidden layers. These layers compute on the data and pass it to the output layer, which then generates the output label. The layers are fully connected with weights (a_{ij}), bias (b_j) and activation function (f) as presented below.

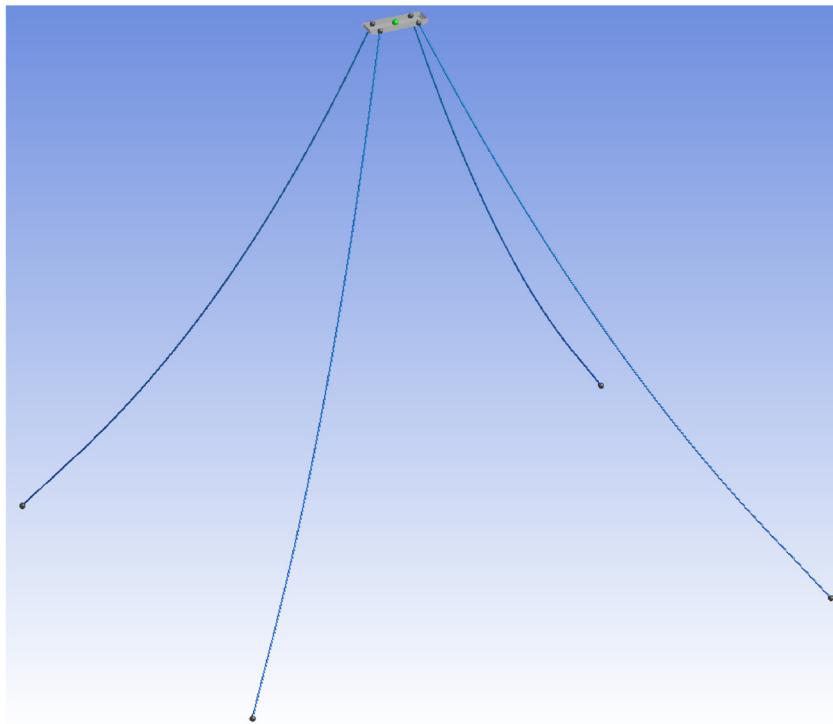
$$Y_j = f(a_{ij}X_i + b_j) \quad (5)$$

where X_i is the input value at the input neuron of i and Y_j is the output value at the output neuron of j . The activation function, denoted by f , determines the output value based on the weighted sum of inputs and bias.

A CNN model utilizes convolutional and pooling layers for feature extraction from input images [27]. The architecture of a typical CNN model is composed of convolutional, pooling, and hidden layers, as presented in Fig. 7(b). To extract relevant features from input images, a typical CNN model employs convolutional and max pooling layers. In detail, input images are fed into the CNN model as feature maps, where each convolutional layer generates output feature maps by applying a filter, kernel and convolutional operator. This process



(a)



(b)

Fig. 4. Hydrodynamic and mooring analysis model. (a) Hydrodynamic panel. (b) Perspective view of mooring system model.

encodes features from the input feature maps into the output feature maps, using zero padding to maintain the shape as the input feature map changes during convolutional operations.

Subsequently, a max pooling layer is employed to extract important features and transfer them to the output feature map. As the convolutional layers deepen, the size of the feature map decreases due to

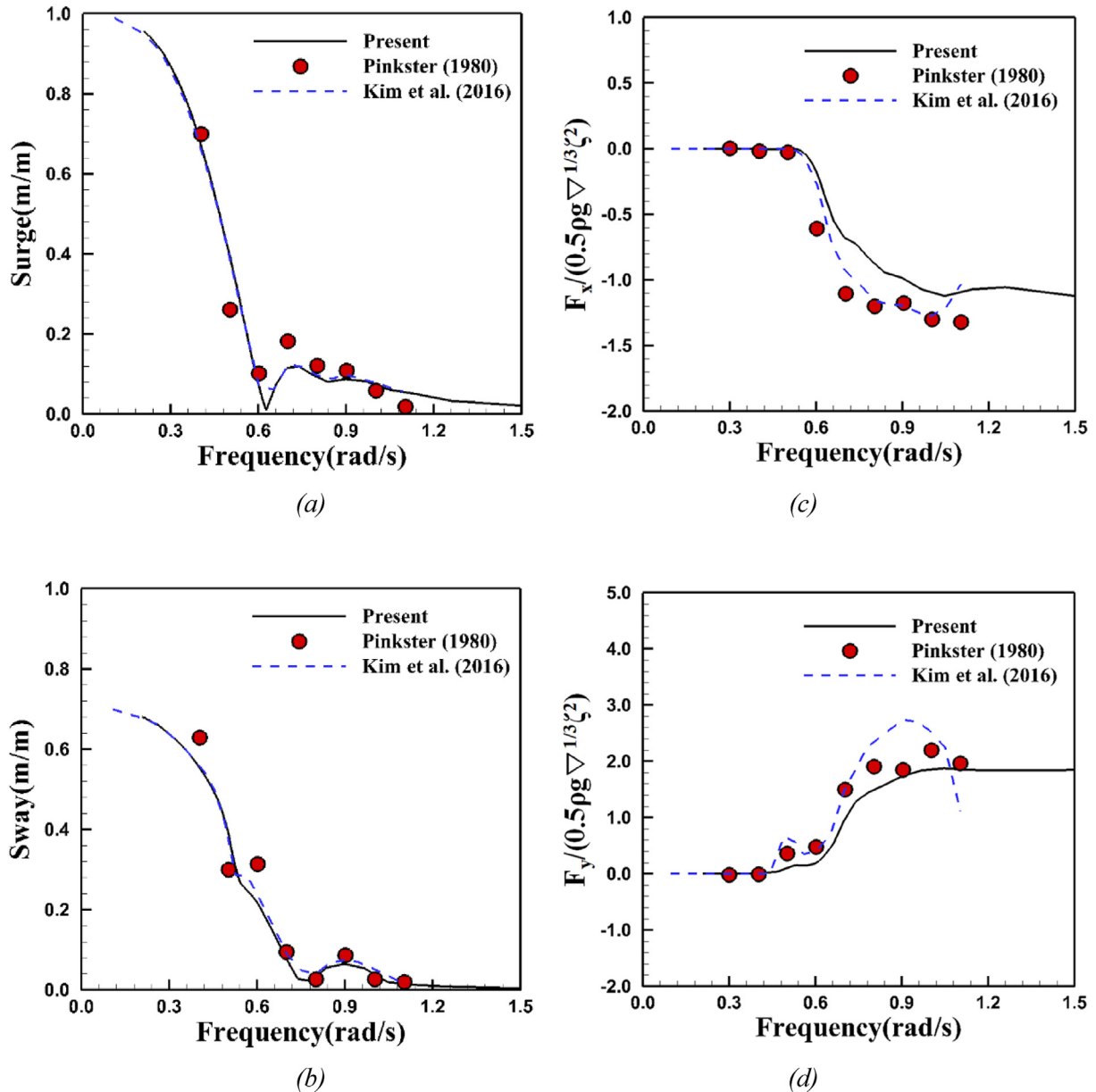


Fig. 5. Comparison of the response amplitude operators and mean drift forces of the barge. (a) Surge RAO in head sea. (b) Sway RAO in beam sea. (c) Surge mean drift force in head sea. (d) Sway mean drift force in beam sea.

the max pooling layer, and more filters are applied. This process enhances the feature extraction and learning capabilities, and it is crucial for effectively managing spatial dimensions and detecting diverse features from the input feature map. The two-dimensional array from the previously convolved and pooled layers is then flattened into a one-dimensional array and connected to hidden layers. The image features extracted by the convolutional layers are processed by the hidden layers and the output of the hidden layers is fed into the output layer to generate the predicted label.

The proposed HNN model simultaneously accepts the input image and input data to enhance the input information as shown in Fig. 7(c). The convolutional layer extracts features from the input image and the extracted features are flattened by the flatten layer. The input data is then concatenated with the flattened feature, and concatenated features are fed into the hidden layers.

The DNN model utilizes 6-DOF motions as input data. The CNN model takes the images of the mooring lines and the barge on the horizontal plane as input data. The HNN model takes both the

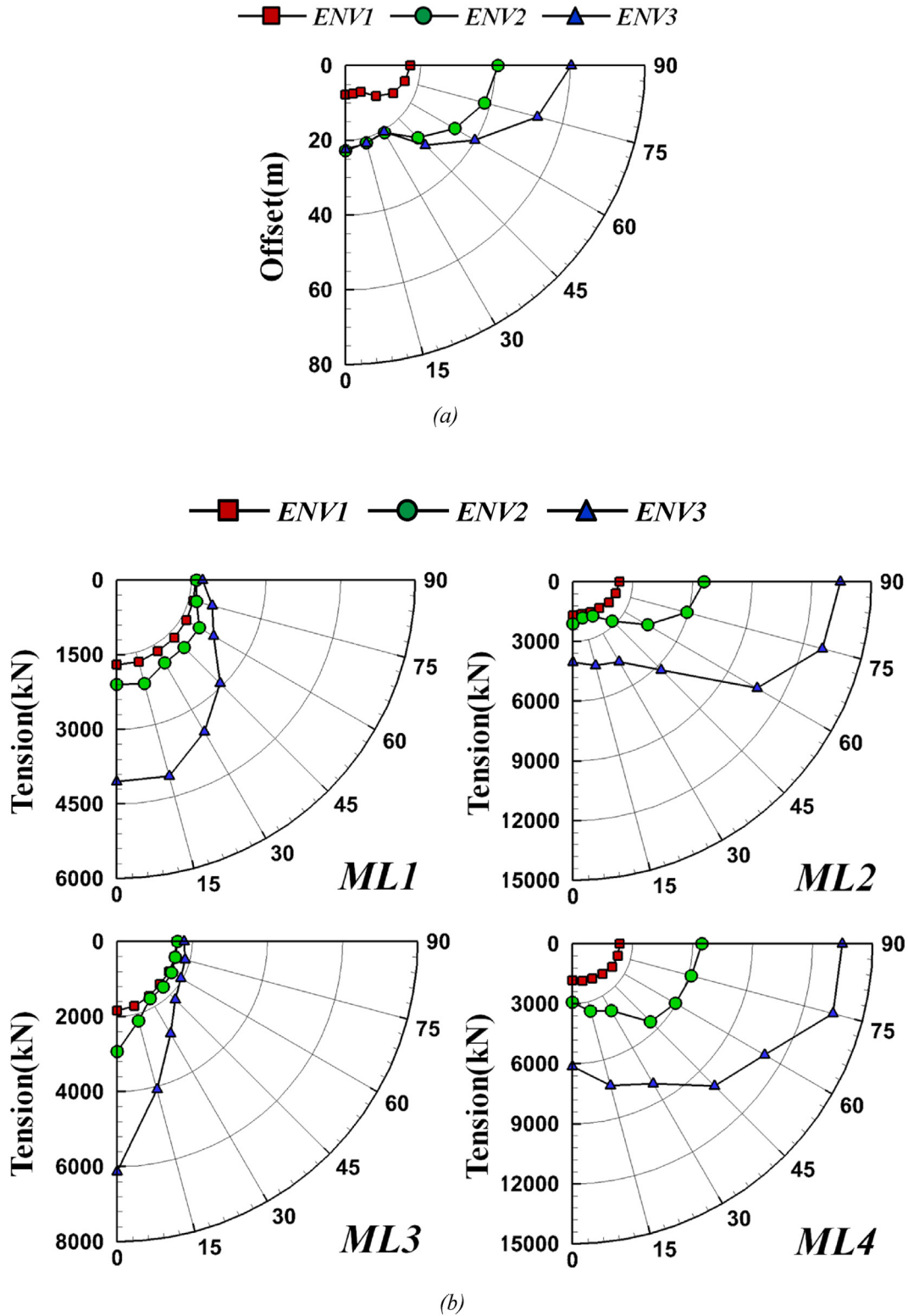


Fig. 6. Summarized results of mooring analysis according to environmental conditions. (a) Offsets of the floating barge. (b) Tensions of mooring lines.

6-DOF motions used in the DNN model and the images used in the CNN model as input simultaneously. The output labels for the three models are identically composed of the axial tension (T) and

inclination (θ) at the fairlead location of each mooring line.

The optimization function used for training is the ADAPtive Moment estimation (ADAM) [28], and the

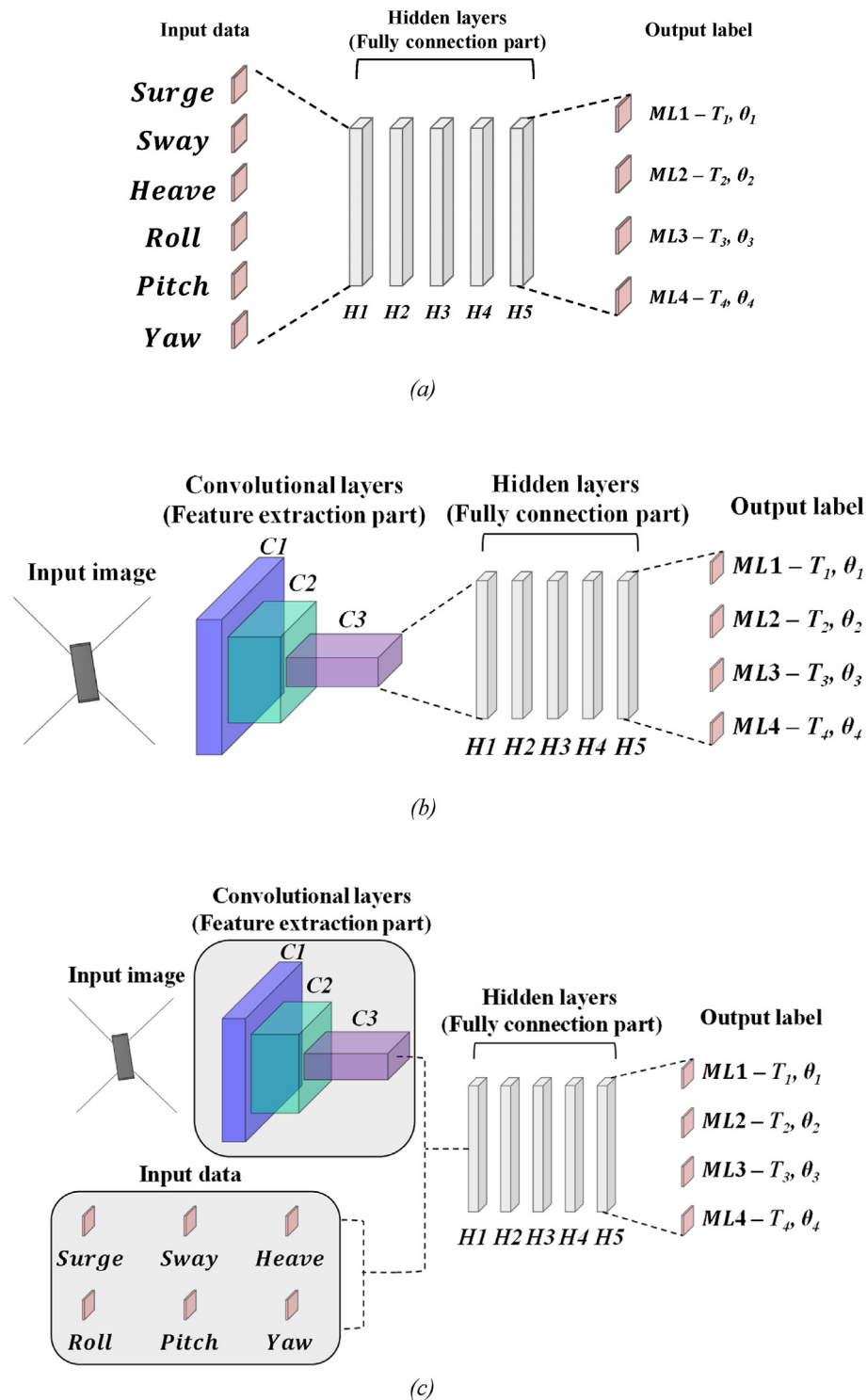


Fig. 7. Typical deep learning models. (a) DNN model. (b) CNN model. (b) HNN model.

Rectified Linear Unit (ReLU) [29] is employed as the activation function. The mean squared error (MSE) is utilized as the loss function for training the models.

$$MSE = \frac{1}{N} \sum_{i=1}^N (Prediction_i - True_i)^2 \tag{6}$$

where, $Prediction_i$ is the predicted value by the deep learning model, $True_i$ is the result value from the analysis and N is the number of dataset.

5. Results and discussion

5.1. Dataset

The dataset used for the deep learning models consists of 6-DOF motions, axial tensions and inclinations of mooring lines extracted every 10 s from the mooring system analysis. Typical input data, input images, and output labels are shown in Fig. 8. The input images used for the CNN and HNN models have a resolution of 512×512 pixels and are zoomed in close to the barge to better visualize its motion (Fig. 8(a)). The dataset consists of 22,680 data samples, which encompass all types and directions of environmental conditions. The data is randomly split into 80% for training and 20% for testing.

5.2. Training of deep learning models

The deep learning models are individually established throughout training. To identify the optimal deep learning model, a comprehensive hyperparameter study is conducted, by systematically adjusting various hyperparameters to optimize their performances.

To investigate the impact of the number of layers on each model, the number of layers in the DNN, CNN, and HNN models is varied as shown in Table 5. For the case of DNN model, the number of hidden layers is varied at 1, 3, and 5. Similarly, for CNN and HNN models, the number of convolutional layers is varied at 1, 3, and 5, while simultaneously varying the number of hidden layers as 1, 3, and 5. The number of neurons in the hidden layer is fixed at 100, while the filter size of the convolutional layers was varied at 32, 64, 128, 256, and 512, respectively, starting from the first layer. Fig. 9 illustrates the changes in the MSE for each model with respect to the epoch. All the models show sufficient convergence at epoch 1000. The DNN model does not show significant differences based on the number of hidden layers. CNN and HNN models show differences based on the number of convolutional layers, with the highest accuracy achieved when there are five convolutional layers. As a result, the DNN model with three intermediate hidden layers, referred to as DH3, and the CNN and HNN models with five convolutional layers and three intermediate hidden layers, referred to as C5H3, are utilized for further study.

In addition to the impact of the number of layers, the effects of the number of neurons are also

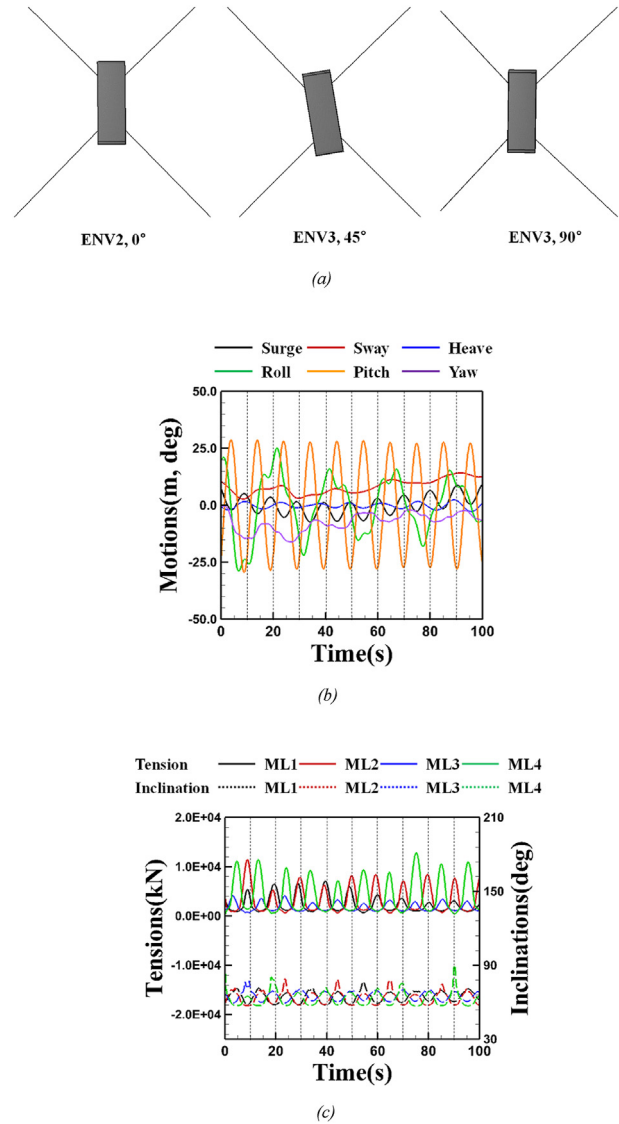


Fig. 8. Typical input images, data and output label from results of time series. (a) Input images. (b) Input data of barge motion. (c) Output label of mooring line tension and inclination.

Table 5. Hyperparameters of number of layers for the training deep learning models.

| Model | Case | Convolution layer | Hidden layer |
|-----------|------|-------------------|--------------|
| DNN | DH1 | — | 1 |
| | DH3 | — | 3 |
| | DH5 | — | 5 |
| CNN & HNN | C1H1 | 1 | 1 |
| | C1H3 | 1 | 3 |
| | C1H5 | 1 | 5 |
| | C3H1 | 3 | 1 |
| | C3H3 | 3 | 3 |
| | C3H5 | 3 | 5 |
| | C5H1 | 5 | 1 |
| | C5H3 | 5 | 3 |
| | C5H5 | 5 | 5 |

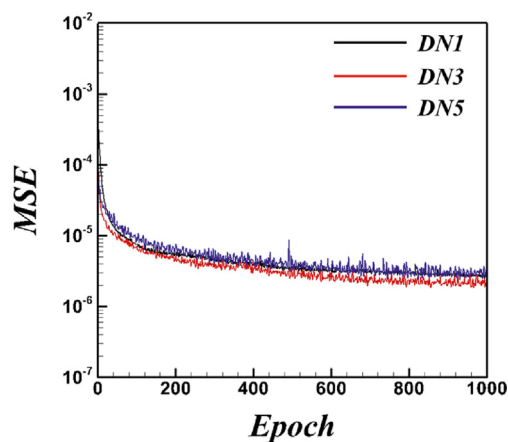
investigated. The number of neurons in the hidden layer is altered, and the filter size of the convolution layer is simultaneously adjusted to investigate their effects. The cases and definitions of the varied hyperparameters are shown in Table 6. Deep learning models are trained for each case, and the MSE values at epoch 1000 are compared in Fig. 10.

For the DNN model, it can be observed that the MSE level is high when the number of neurons is small, and gradually converges to a lower value with an increase in the number of neurons as shown in Fig. 10(a). CNN and HNN models also converge to a lower MSE level by capturing the image features well as the number of filter and hidden layer increase, as shown in Fig. 10(b) and (c). As a result, the DH3-N3 architecture is selected as a representative for the DNN model and the C5H3-N3 architecture is selected as the representative for the CNN and HNN models, both demonstrating the lowest MSE levels. These established models are then utilized for testing and prediction in further study.

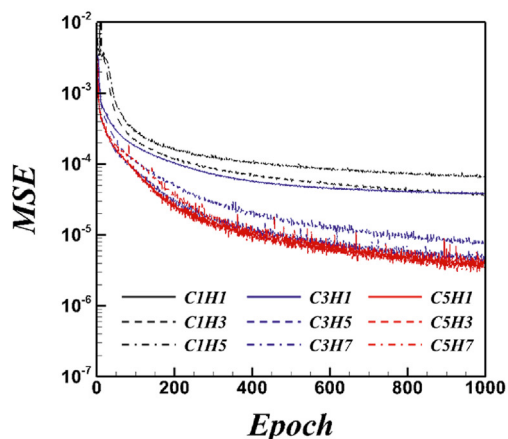
5.3. Test of deep learning models

In test stage, the mooring line tension and inclination are predicted using the established deep learning models. The 6804 pieces of test data that are not used for training are utilized. The tensions and inclinations predicted by the DNN model are compared with true values as presented in Fig. 11. The solid lines and points represent the true and predicted values, respectively. It can be observed that most of the predicted values are clustered near the true values indicated by the 45° angle. This demonstrates the high accuracy of the established DNN model in predicting mooring line tension and inclination. In the region with high tension, some predicted values show an increasing difference from the true values. This is because the number of data is relatively small compared to that of the region with low tension, which lowers the prediction accuracy by the DNN (Fig. 11(b)). In the case of inclination, it can be observed that the values are distributed marginally closer to the true value compared to tension (Fig. 11(e), (f)).

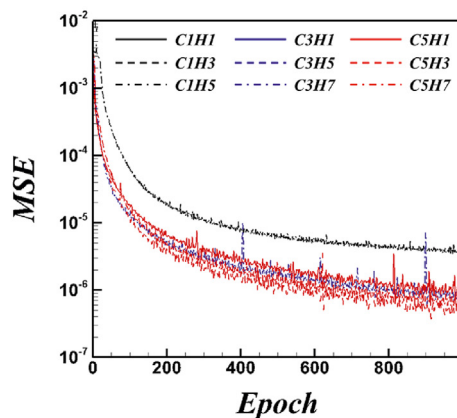
The prediction results using the CNN model are presented in Fig. 12. Overall, the predicted values of the CNN model are distributed in a similar location to that of the true value. However, they are more scattered from the true value compared with the DNN model as shown in Fig. 11. It is evident that the distribution of the points becomes wider and the error increases as the tension increases, especially compared to the low tension range (Fig. 12(a), (d)). This increase in error is because the input image



(a)



(b)



(c)

Fig. 9. Convergence histories of MSE by hyperparameter study of the number of layers. (a) DNN model. (b) CNN model. (c) HNN model.

only represents the features of the barge motion and line arrangement on the horizontal plane, as shown in Fig. 8(a), and consequently does not adequately capture features related to the heave, roll, and pitch.

Table 6. Hyperparameters of the number of neurons and filters for the training deep learning models.

| Model | Case | Number of neurons (Hidden layers) | Filters (1st-2nd-3rd-4th-5th convolutional layer) |
|-------|-----------|--------------------------------------|---|
| DNN | DH3-N1 | 10 | — |
| | DH3-N2 | 50 | — |
| | DH3-N3 | 100 | — |
| CNN | C5H3-N1 | 10 | 8-16-32-64-128 |
| | & C5H3-N2 | 50 | 16-32-64-128-256 |
| HNN | C5H3-N3 | 100 | 32-64-128-256-512 |

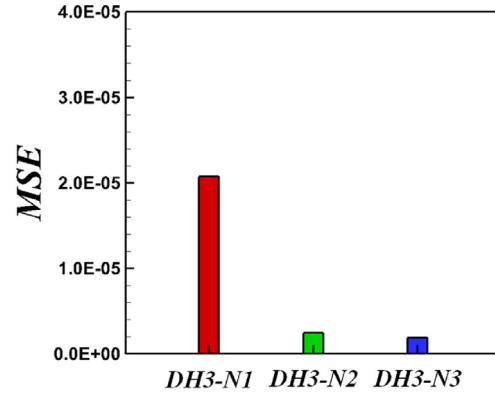
In contrast, the DNN model can reflect the motion characteristics excluded in the CNN model because it uses all the 6-DOF motions as input data. Additionally, the scatter of the mooring line inclination is also more broadly distributed than that of the DNN model.

The prediction results of the HNN model, which consolidates the characteristics of the DNN and CNN models, are in good agreement with the true value, similar to the DNN results as shown in Fig. 13. Most of the points are close to the 45° line. These results confirm that 6-DOF motions are dominant in estimating the tension and inclination of the mooring system.

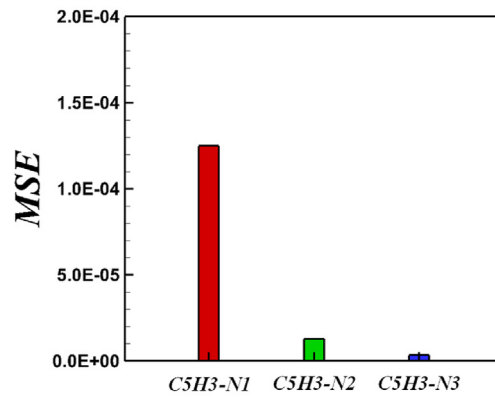
To quantitatively compare the errors of the three models, the cumulative error of the predicted values of each model is presented in Fig. 14. The cumulative error is represented as the average of the relative differences between the true values and predicted values of all the mooring lines. In the case of tension, the model with the lowest error is HNN, and 80% of the test dataset shows an error of less than 1%. For the DNN and CNN models, about 80% of the test dataset has an error of less than 2% and 7%, respectively. The inclination is more accurate than the tension, and DNN and HNN mostly have an error of less than 1%, whereas approximately 80% of the test dataset for the CNN model has an error of less than 2%. The higher prediction accuracy of inclination compared to tension is attributed to the relatively narrow range of the dataset and the more even distribution of data within the range. As a result, both the established DNN and HNN models predict the characteristics of the mooring line well.

5.4. Prediction of mooring characteristics for other environments

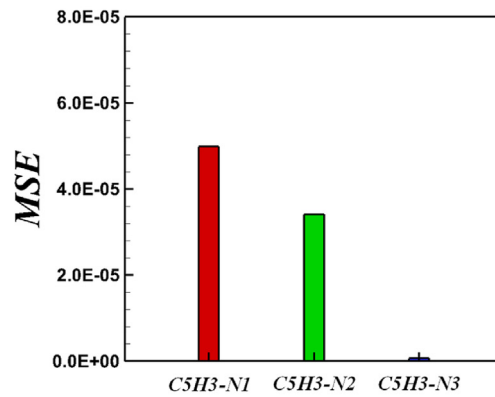
To verify the applicability of the established deep learning model as a monitoring system, the tension and inclination of the mooring line are predicted for ENV4, ENV5, and ENV6, which are not used for training and testing as shown in Table 4. ENV4 is



(a)



(b)



(c)

Fig. 10. Convergence levels of MSE by hyperparameter study of the number of neurons and filters. (a) DNN model. (b) CNN model. (c) HNN model.

selected as a benign environment, while ENV5 represents the median environment among those used for training and testing. ENV6 is the harshest environment among all the environmental

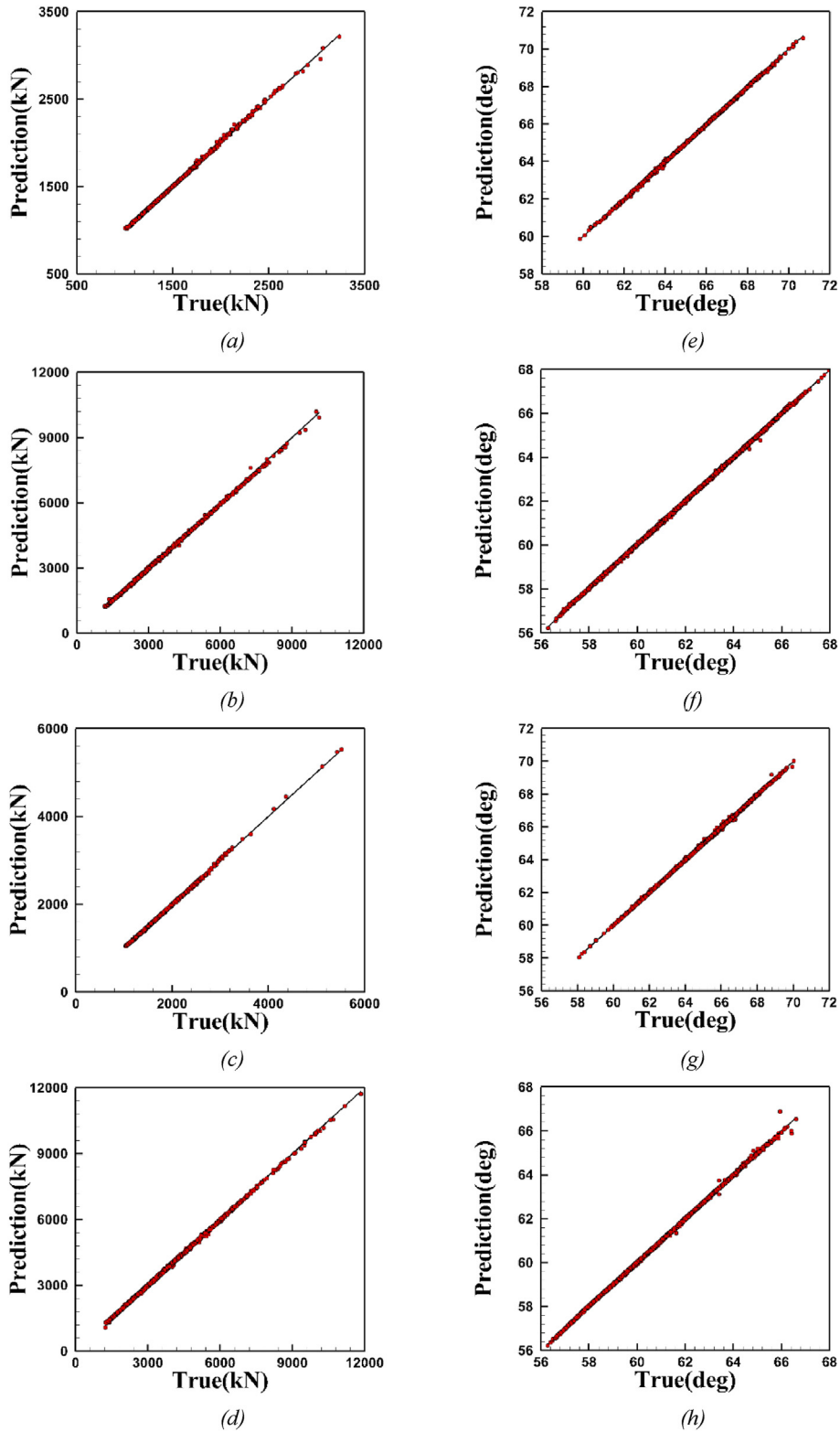


Fig. 11. Comparison of true and predicted values for DNN model. (a) T_1 . (b) T_2 . (c) T_3 . (d) T_4 . (e) θ_1 . (f) θ_2 . (g) θ_3 . (h) θ_4 .

conditions, and it is a condition outside of the training and test environment conditions. The established DNN and HNN models are considered, which have high prediction accuracy during the test.

Fig. 15 shows the distribution of true and predicted values by the DNN and HNN models for ENV4, ENV5 and ENV6. The red bars represent the true values obtained through analysis, while the

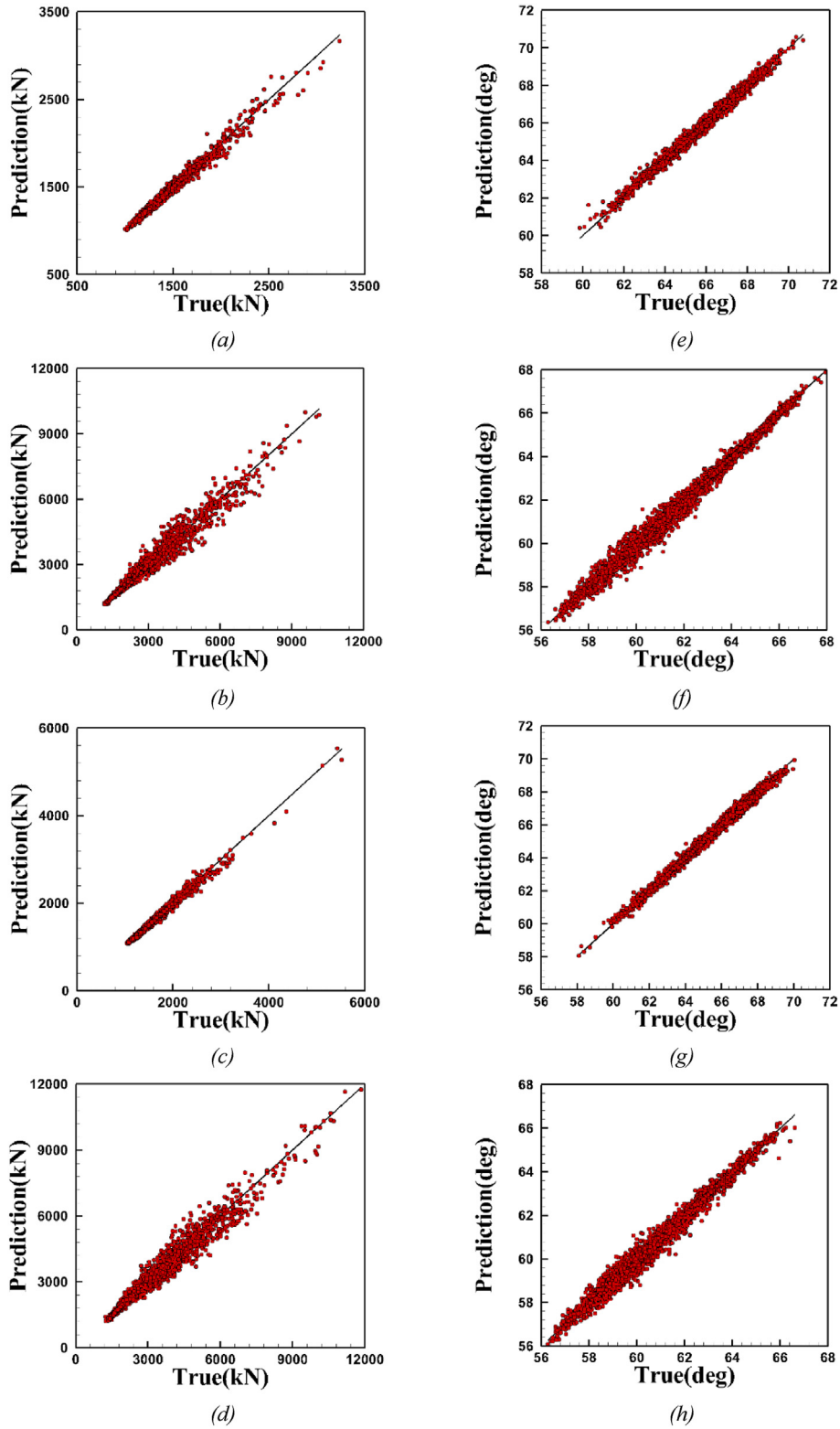


Fig. 12. Comparison of true and predicted values for CNN model. (a) T_1 . (b) T_2 . (c) T_3 . (d) T_4 . (e) θ_1 . (f) θ_2 . (g) θ_3 . (h) θ_4 .

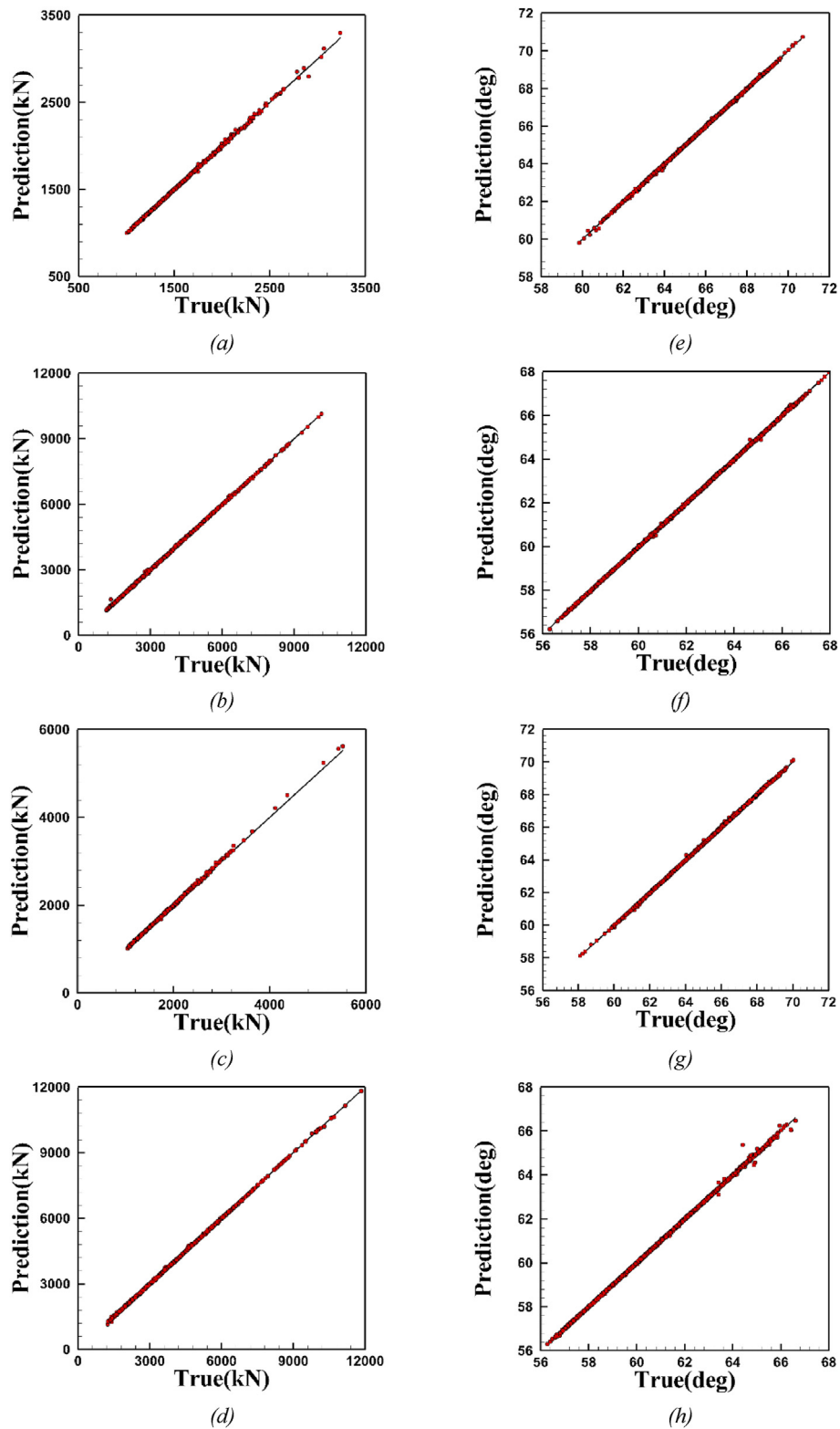
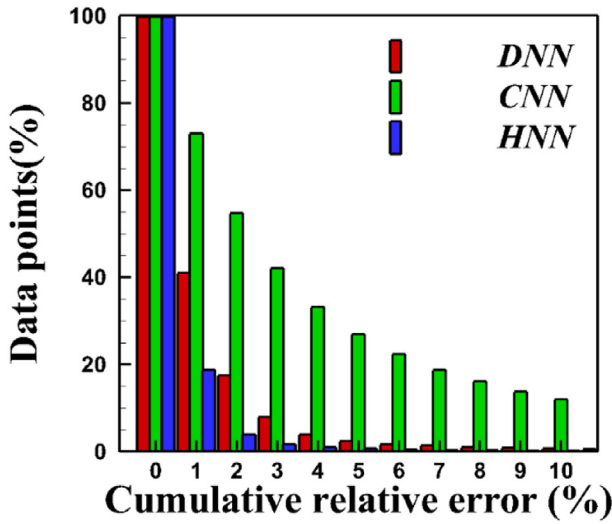


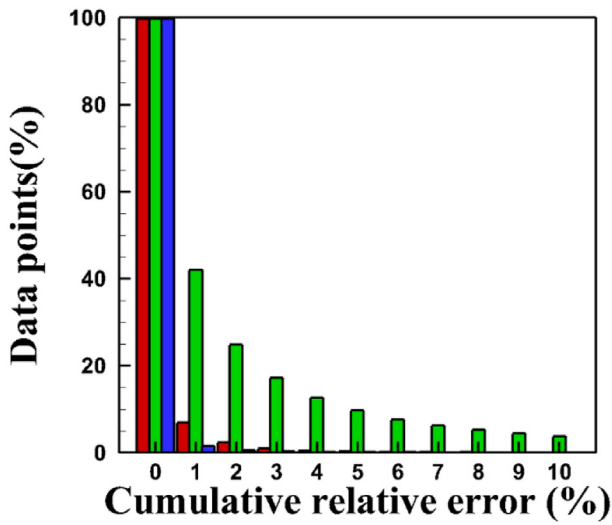
Fig. 13. Comparison of true and predicted values for HNN model. (a) T_1 . (b) T_2 . (c) T_3 . (d) T_4 . (e) θ_1 . (f) θ_2 . (g) θ_3 . (h) θ_4 .

solid and dashed lines represent the predicted values from the DNN and HNN models, respectively. For ENV4, the distribution of predicted tensions using the DNN model shows a difference

from the distribution of the true tension values at the location where the most data is distributed, but overall distribution of the predicted tensions is similar to that of the true values. It can be



(a)



(b)

Fig. 14. Distributions of data points with cumulative relative error. (a) Averaged tensions. (b) Averaged inclinations.

confirmed that the inclination prediction results are better matched than the distribution of the tensions. This is because the prediction accuracy of both models is higher for inclination, as shown in the test results (Fig. 14). In the case of ENV5 and ENV6, there is almost no noticeable difference in the distribution between true and predicted values, which holds true for both tension and inclination (Fig. 15 (b), (c)).

Based on the test results, it is evident that the prediction accuracy is relatively low in the high tension range, which corresponds to a relatively small dataset. This trend is not readily apparent from the distribution of the entire dataset depicted

in Fig. 15. Therefore, the true and predicted values for individual mooring lines under each environmental condition are compared using time histories, and the results are shown in Figs. 16–18. During the simulation, we examine data from 8000 s to 10,000 s, which represents a sufficiently developed period of environmental conditions and changes in mooring lines.

As illustrated in Fig. 6, the conditions under which the mooring lines experience the maximum tension are dependent on the direction of the environmental conditions. For ML1 and ML3, the maximum mooring line tension occurs when the environmental loads are applied at 0°, while for ML2 and ML4, it occurs at 90°. Based on this trend, the representative conditions for each mooring line under which the maximum environmental loads are applied are presented in Figs. 16–18.

For ENV4, the difference in the tension between the mooring lines under different environmental directions is not significant, as shown in Fig. 16. The mooring line tension and inclination are close to the true values in ENV4. However, a slight shift is observed in the mooring line tension predicted by the DNN model in ML4 (Fig. 16(d)). This trend explains the result of the distribution of tension is being shifted to the lower part as shown in Fig. 15(a). Similar trends can be seen in the tension of other mooring lines, but the quantity of difference is not significant as the environmental condition is benign.

The true and predicted values for ENV5 are shown in Fig. 17. ML2 and ML4 exhibit high average and peak mooring line tension at an environmental direction of 90° compared with those of other directions. This is attributed to their increased projection area, which proportionally amplifies the load exerted by wind and current. In contrast, ML1 and ML3 experience relatively lower tension. Overall, the prediction results closely align with the true values depending on the mooring lines. In particular, there is negligible variance between the true and predicted values at the peaks of tension and inclination. This can be attributed to the median environmental condition falling between the conditions used for training and testing.

As depicted in Fig. 18, there are discrepancies between the predicted tension values and the true values for several peaks in the ENV6 results. At peak points, the excessive motion and positioning of the floating barge occur, and such input data are not included in the training of the DNN and HNN models. As a result, at locations where excessive mooring line tension and inclination occur, the predictions of the trained models deviate from the true values. However, except for some peak points,

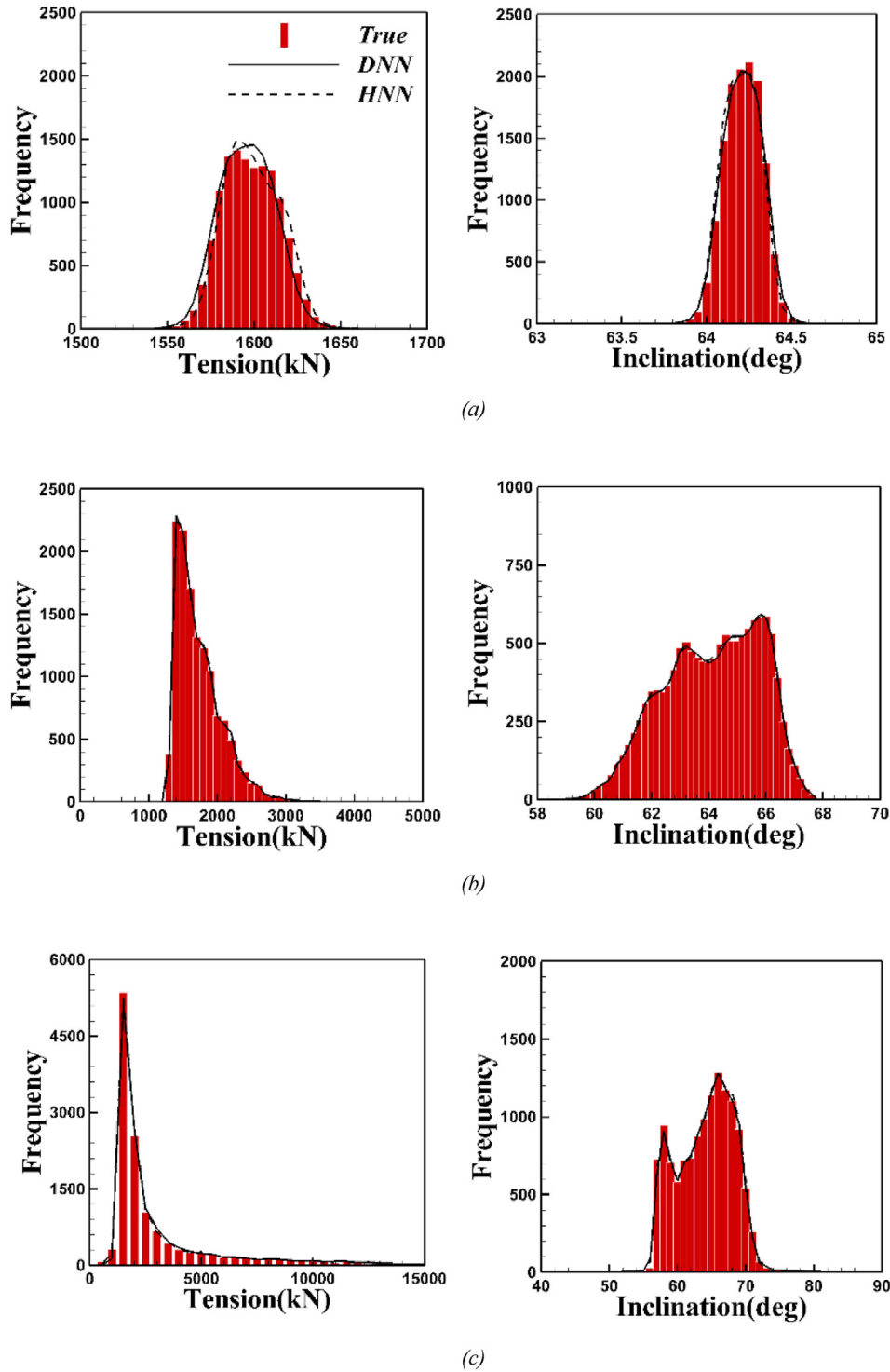


Fig. 15. Histogram of mooring tensions (left column) and inclinations (right column). (a) ENV4. (b) ENV5. (c) ENV6.

it can be observed that the tension and inclination predicted through the DNN and HNN models generally align well with the true values, even when considering environments that are not used in the training of the deep learning models. In conclusion,

to improve the accuracy and applicability of the deep learning models in predicting the characteristics of mooring lines, it is essential to select data that cover the environmental conditions of the operating area.

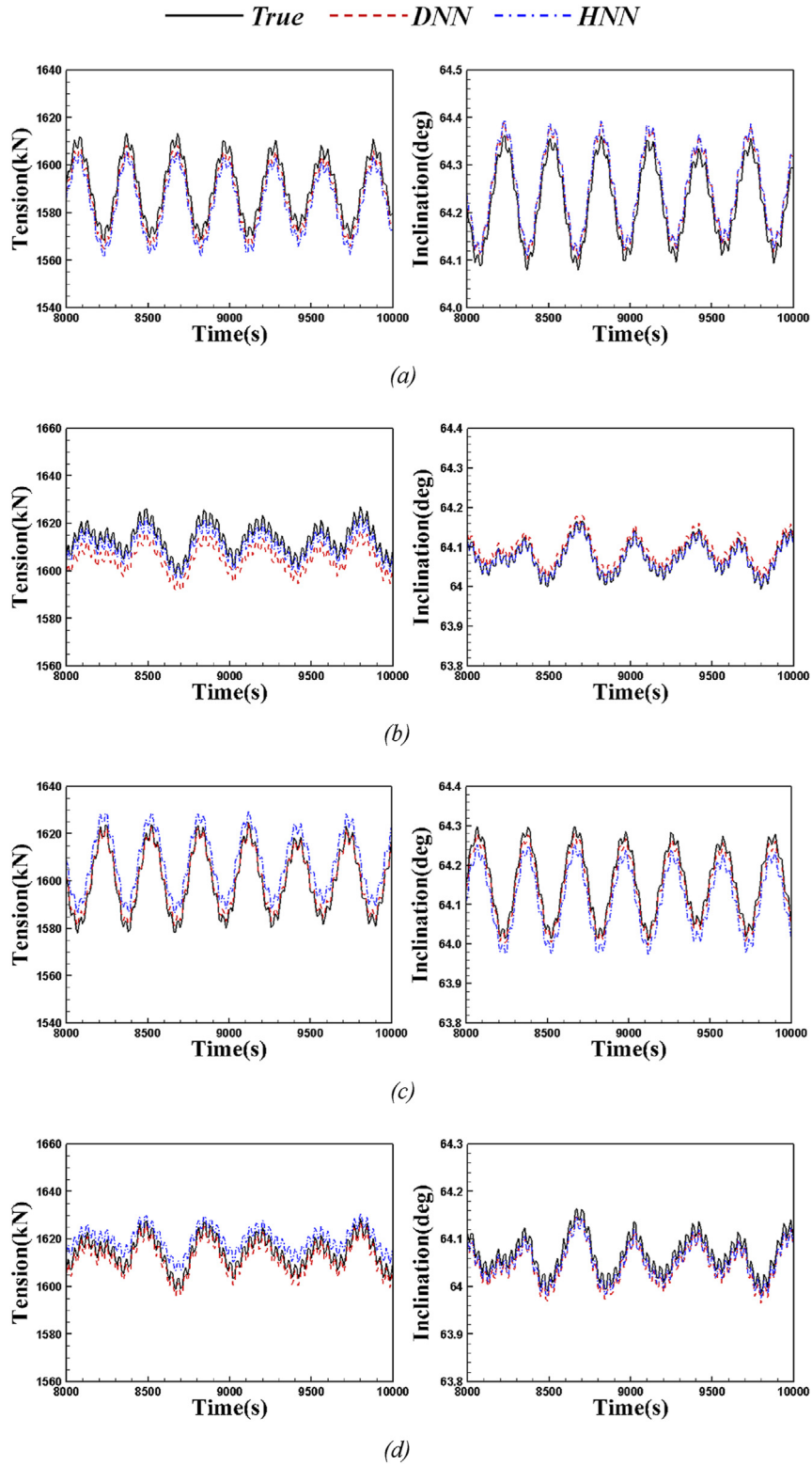


Fig. 16. Predicted tensions (left column) and inclinations (right column) for ENV4 condition. (a) ML1 at 0° environmental direction. (b) ML2 at 90° environmental direction. (c) ML3 at 0° environmental direction. (d) ML4 at 90° environmental direction.

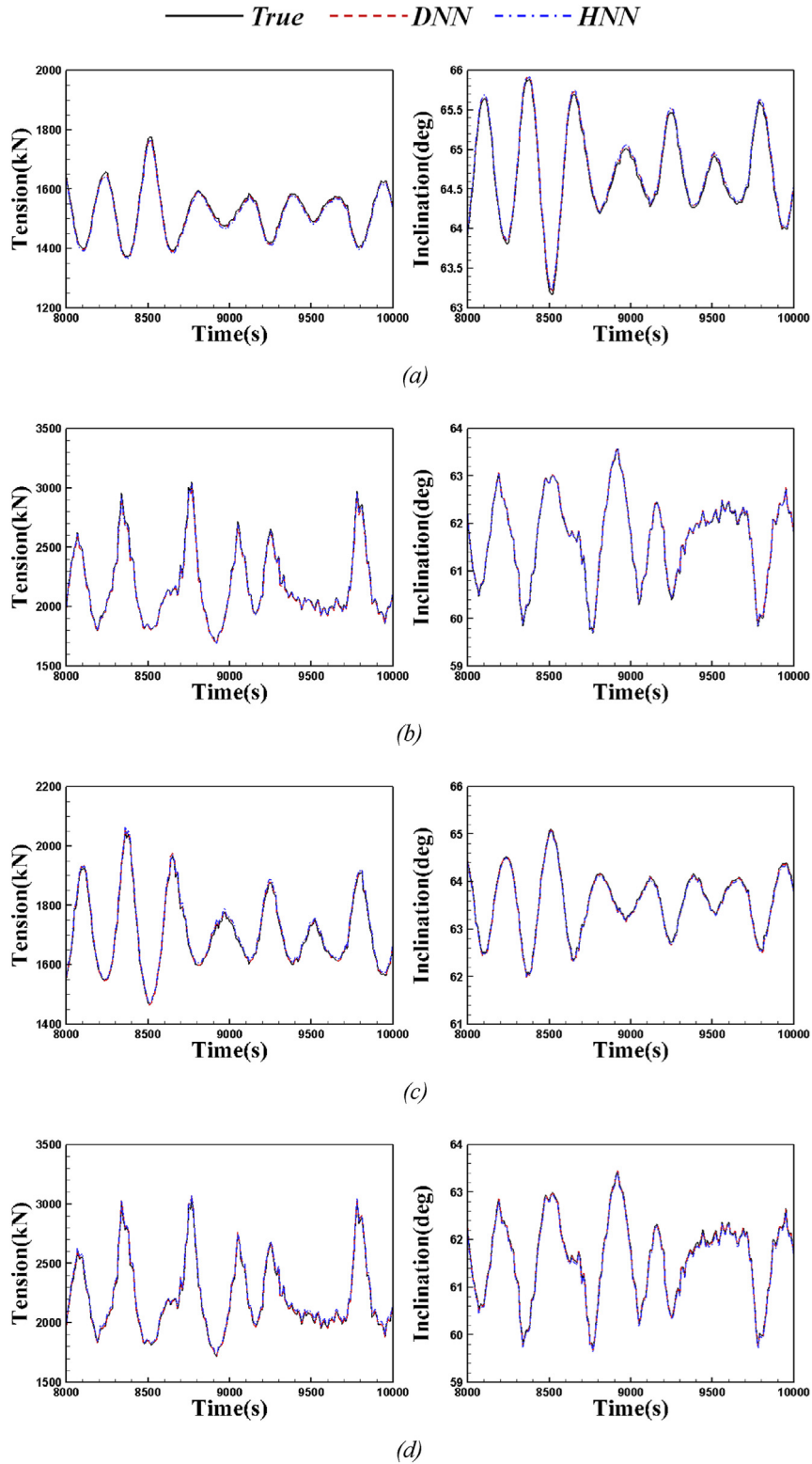


Fig. 17. Predicted tensions (left column) and inclinations (right column) for ENV5 condition. (a) ML1 at 0° environmental direction. (b) ML2 at 90° environmental direction. (c) ML3 at 0° environmental direction. (d) ML4 at 90° environmental direction.

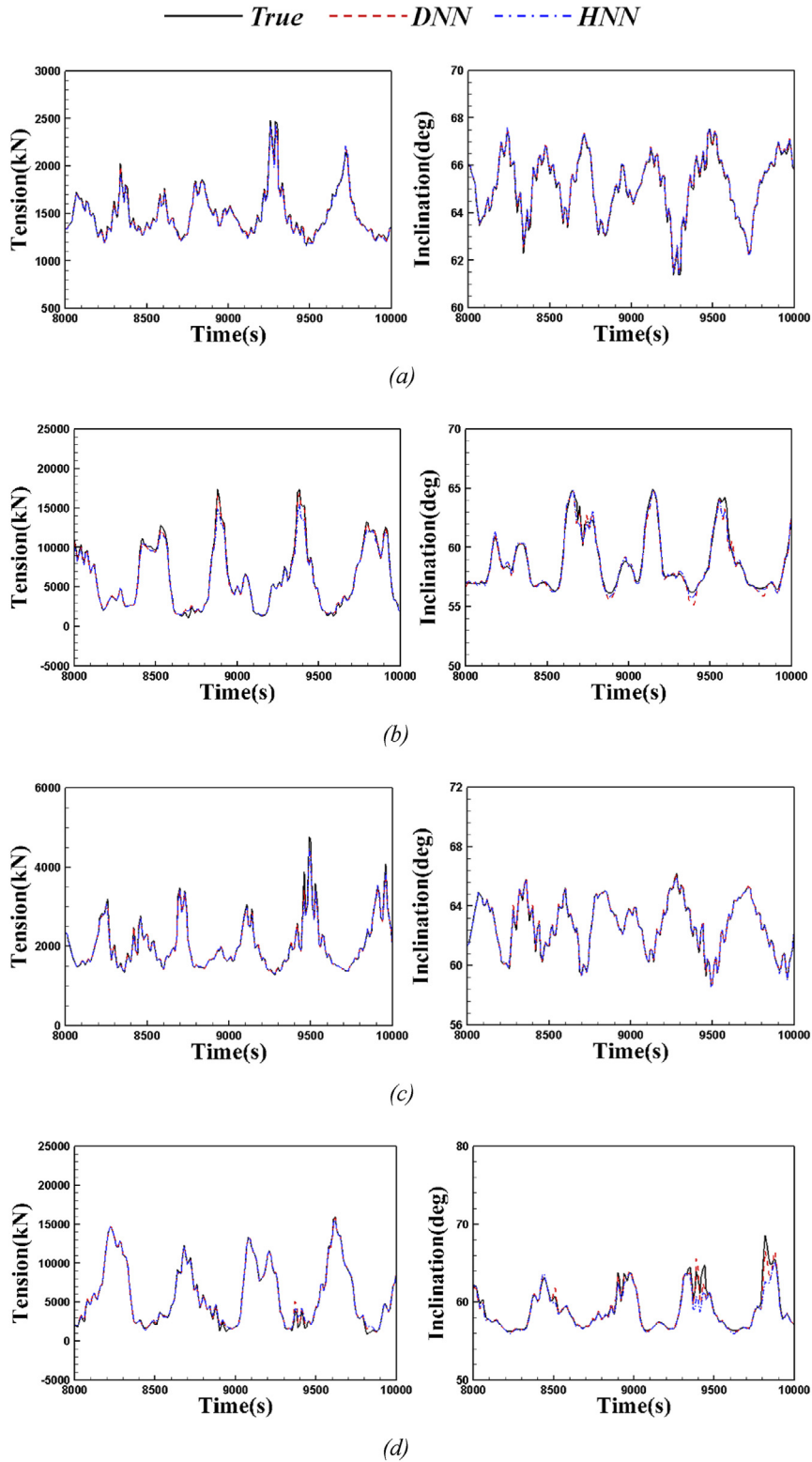


Fig. 18. Predicted tensions (left column) and inclinations (right column) for ENV6 condition. (a) ML1 at 0° environmental direction. (b) ML2 at 90° environmental direction. (c) ML3 at 0° environmental direction. (d) ML4 at 90° environmental direction.

6. Conclusions

The present study establishes three deep learning models to predict line tension and inclination of the mooring systems of a floating barge. The first model is DNN that takes into account the 6-DOF motion values of the floating barge as input data. The second model is CNN that uses images of the floating barge and mooring lines in the horizontal plane as input data. The final model, referred to as the HNN model, consolidates the input data from the DNN and CNN models. The output labels are defined as axial tension and inclination for four mooring lines. To construct a dataset for the deep learning models, hydrodynamic and mooring analyses of the floating barge are conducted.

A hyperparameter study is conducted to train the three models. Initially, the number of layers is adjusted to observe the change in the loss function of MSE. Subsequently, variations are made to the number of neurons in the hidden layer and the number of filters in the convolutional layer to establish the model with the highest accuracy.

The predictive accuracy of the three models is evaluated by testing phase. While the DNN and HNN models show similar prediction results to the true values, the CNN model is found to have a relatively lower accuracy. This is because the input data for the CNN model is images of the horizontal plane, which do not reflect the characteristics of heave, roll and pitch motions. Additionally, the accuracy is low for all the models in the high tension region where the amount of data is relatively small, and the prediction accuracy of inclination is higher than tension where the data is relatively evenly distributed.

To verify the applicability of the established models, mooring line tension and inclination predictions are performed under environmental conditions which are not used in training and testing, and compared with the true values. The overall distributions of the true and predicted tension and inclination are compared, and it is confirmed that most of the overall distributions are well matched.

Additionally, a comparison of the true and predicted values is performed using time history, and it is confirmed that the predicted values are slightly shifted under the benign condition. Under median conditions, the overall predicted values show good agreement with the true values. Under harsh conditions, there are differences in several peaks between the true values and predicted values. This is because the established DNN and HNN models are not trained for excessive mooring line tension and inclination.

The calculation times for the training and testing of the DNN and HNN models, using the same resources and graphic processing unit (GPU), are approximately 0.5 and 6.0 hours, respectively. This difference in training time is attributed to the input data and model architecture. The DNN model receives scalar inputs and employs simple architectures. In contrast, the HNN model utilizes image inputs and includes multiple convolutional layers in its architecture for extracting image features. However, the time required for prediction using established deep learning models is not significant for the DNN and HNN models.

Through this study, it is confirmed that the deep learning models for predicting the characteristics of mooring systems need to consider a suitable range of environmental conditions. Additionally, it is evident that there are limitations to relying solely on input images from the horizontal plane. Furthermore, when combining input images with 6-DOF data, we obtain more accurate prediction results. The proposed deep learning models, utilizing information obtained from the floater at the operating site, are expected to sufficiently replace the mooring monitoring system with highly accurate real-time predictions of mooring line tension and inclination. Additionally, the use of the proposed deep learning models as a mooring monitoring system is expected to reduce the costs associated with establishing analysis software and address maintenance issues. Since the present study only considers a simple floating barge with four mooring lines, the applicability of the deep learning model to future spread and turret mooring systems, which involve clustering multiple mooring lines, should be investigated.

Ethical information

This study did not involve any human or animal subjects, thus ethical approval was not required.

Conflict of interest

There is no conflict of interest.

Acknowledgements

This work was supported by the establishment of software predicting roll motion and safety of fishing vessel based on D.N.A. grant funded by the Korea Maritime transportation Safety Authority (KOMSA).

References

- [1] Norske Veritas Det. DNV-OS-E301 position mooring. 2021.

- [2] American Bureau of Shipping. Guidance notes on mooring integrity management. 2018.
- [3] Ormberg H, Larsen K. Coupled analysis of floater motion and mooring dynamics for a turret-moored ship. *Appl Ocean Res* 1998;20(1–2):55–67.
- [4] Low YM, Langley RS. Time and frequency domain coupled analysis of deepwater floating production systems. *Appl Ocean Res* 2006;28(6):371–85.
- [5] Garrett DL. Dynamic analysis of slender rods. 1982.
- [6] Davies KB, Mungall JCH. Methods for Coupled Analysis of TLP's. In: *Offshore Technology conference*; 1991. OTC-6567.
- [7] Kim BW, Sung HG, Kim JH, Hong SY. Comparison of linear spring and nonlinear FEM methods in dynamic coupled analysis of floating structure and mooring system. *J Fluid Struct* 2013;42:205–27.
- [8] Vázquez-Hernández AO, Sudati Sagrilo LSV, Ellwanger GB. On the extreme analysis applied to moored floating platforms. *Int Conf Offshore Mech Arctic Eng* 2003; 36819:241–7.
- [9] Stanisic D, Efthymiou M, Kimiaei M, Zhao W. Evaluation of conventional methods of establishing extreme mooring design loads. *Int Conf Offshore Mech Arctic Eng* 2017: 57656.
- [10] Sagrilo LSVS, Naess A, Gao Z. On the extreme value analysis of the response of a turret moored FPSO. *J Offshore Mech Arctic Eng* 2012;134(4).
- [11] Simoes MG, Tiquilloca JLM, Morishita HM. Neural-network-based prediction of mooring forces in floating production storage and offloading systems. *IEEE Trans Ind Appl* 2002;38(2):457–66.
- [12] Guarize R, Matos NAF, Sagrilo LVS, Lima ECP. Neural networks in the dynamic response analysis of slender marine structures. *Appl Ocean Res* 2007;29(4):191–8.
- [13] de Pina AC, da Fonseca Monteiro B, Albrecht CH, de Lima BSLP, Jacob BP. ANN and wavelet network meta-models for the coupled analysis of floating production systems. *Appl Ocean Res* 2014;48:21–32.
- [14] de Pina AA, da Fonseca Monteiro B, Albrecht CH, de Lima BSLP, Jacob BP. Artificial Neural Networks for the analysis of spread mooring configurations for floating production systems. *Appl Ocean Res* 2016;59:254–64.
- [15] Christiansen NH, Voie PET, Winther O, Høgsberg J. Comparison of neural network error measures for simulation of slender marine structures. *J Appl Math* 2014;759834.
- [16] Mentas A, Yetkin M, Kim Y. Comparison of ANN and ANFIS techniques on modelling of spread mooring systems. In: *Proceedings of the 30th asian-pacific technical exchange and advisory meeting on Marine structures*; 2016.
- [17] Uddin M, Jameel M, Razak HA, Islam ABM. Response prediction of offshore floating structure using artificial neural network. *Adv Sci Lett* 2012;14(1):186–9.
- [18] Yetkin M, Mentas A. Optimization of spread mooring systems with Artificial Neural Networks. *Towards Green Marine Technology and Transport* 2015:233–8.
- [19] Sidarta DE, Kyoung J, O'Sullivan J, Lambrakos KF. Prediction of offshore platform mooring line tensions using artificial neural network. In: *International conference on offshore mechanics and arctic engineering*; 2017. p. 57632.
- [20] Chung M, Kim S, Lee K. Detection of damaged mooring line based on deep neural networks. *Ocean Eng* 2020;209:107522.
- [21] Lee K, Chung M, Kim S. Damage detection of catenary mooring line based on recurrent neural networks. *Ocean Eng* 2021;227:108898.
- [22] Saad AM, Schopp F, Barreira RA, Santos IH, Tannuri EA, Gomi ES, Costa AHR. Using Neural Network Approaches to Detect Mooring Line Failure. *IEEE Access* 2021;9:27678–95.
- [23] Pinkster JA. Low-frequency phenomena associated with vessels moored at sea. *Soc Petrol Eng J* 1975;15(6):487–94.
- [24] Oil Companies International Marine Forum. Mooring equipment guidelines. 2008.
- [25] Bureau Veritas. Classification of mooring systems for permanent offshore units. 2021. NR 493 DT R04 E.
- [26] Kim MS, Jung KH, Park SB. Wave induced coupled motions and structural loads between two offshore floating structures in waves. *Brodogradnja* 2018;69(3):149–73.
- [27] LeCun Y, Bengio Y, Hinton G. Deep learning. *Nature* 2015; 521(7553):436–44.
- [28] Kingma DP, Ba J. Adam: a method for stochastic optimization. 2014. arXiv preprint arXiv:1412.6980.
- [29] Nair V, Hinton GE. Rectified linear units improve restricted boltzmann machines. In: *Proceedings of the 27th international conference on machine learning. ICML-10*; 2010. p. 807–14.